EXPERIMENTAL DYNAMIC STALL STUDY OF AN AIRFOIL IN TURBULENT FLOW

J. MARAÑON DI LEO[†‡], J. S. DELNERO[†‡] and S. ALGOZINO[†‡]

† *UIDET-LaCLyFA: Unidad de Investigación, Desarrollo, Extensión y Transferencia – Capa Límite y Fluidodinámica Ambiental, Facultad de Ingeniería, UNLP. Calle 116 e/47 y 48 (1900), La Plata, Bs. As., Argentina.*
‡ *CONICET: Consejo Nacional de Investigaciones Científicas y Técnicas, Avda. Rivadavia 1917, CP C1033AAJ, Ciudad Autónoma de Buenos Aires, Argentina. E-mail: jmaranon@ing.unlp.edu.ar*

***Abstract*— The objective of this study is to experimentally determine the fluid dynamic configuration of the dynamic stall of an airfoil in turbulent flow. Wind tunnel tests were carried out in order to characterize the airfoils behavior in static and static after a quick change in the angle of attack ("dynamic case") using flow visualization, loads and hot-wire anemometry measurements at different Reynolds numbers and with one rate of change for the angle of attack. In all the tests, a Worthmann FX 63-137 airfoil model was used. First, with the visualizations made using a paint technique, for the different configurations, some differences in the flow pattern were found and points of interest in the airfoil were chosen. In those points, the sensors for the velocity measurements were placed. With the velocities acquired using a hot-wire system, autocorrelations, turbulence intensities, density power spectrums and wavelet maps were calculated and compared between the static and the dynamic case; different results were found and explained. Additionally, differences were traced in the turbulent intensities in the wake of the airfoil. Furthermore, a wavelets analysis was performed, and the flow scales obtained show differences for the same conditions analyzed before.**

***Keywords*— Wind tunnel, Aerodynamic, Detachments, Re-circulatory, Hot-wire anemometry.**

NOMENCLATURE

C = Chord length of the model
$C(t)$ = Autocorrelation coefficient
C_l = Lift coefficient
f = Frequency (Hz)
PSD = Power Spectral Density
Re = Reynolds number
R_u = Autocorrelation function
$S(f)$ = Density Power Spectra
T = Measurement period
t = time
u, v = Longitudinal and vertical velocity component
u', v' = Fluctuation of the u and v velocity
V = Reference velocity
α = angle of attack
λ_s = Integral turbulent spatial scale
λ_t = Integral turbulent temporal scale
σ^2_u = Variance of u
ρ = density

I. INTRODUCTION

The existence of more than one solution for the flow pat-tern around an airfoil, operating at a given angle of attack in the stall zone, can be studied by the "large angle of attack aerodynamics" and their associated mechanisms.

Flow separation phenomena are common in aircraft operating under several different scenarios: high angles of attack, steep turns, aerobatics flight, aircraft flying in turbulent atmospheres, flight over aircraft wake, wing interacting with vortices, helicopter rotors disturbed by atmospheric turbulence or in the wake of preceding blade and wind turbines.

The static stall angle of attack is the minimum angle at which a statically exposed airfoil to a uniform flow begins to show the stall phenomena. Starting with small angles of attack, the lift typically grows linearly as the angle of attack increases. It is generally accepted that the stall angle is the first angle for which there is a significant deviation from this linear relationship. This should be considered merely as a practical definition, because physically, this deviation from the linear behavior is not necessarily associated neither with the beginning of the actual flow separation process nor with the change in flow pattern that characterizes a stall (Elkhoury *et al*., 2008; Hui and Zifeng, 2008). As known, according to different geometrical airfoil characteristics and the oncoming flow profiles, the stall, or its associated mechanisms, are different. Flow separation on the airfoil can occur when the angle of attack is large enough to cause a re-circulatory bubble to explode after moving from the leading to the trailing edge, generating the stall. Another cause for flow separation is when a bubble stays in the leading edge zone and grows enough to cause a soft stall from flow separation on the trailing edge. All this clearly depends on the Reynolds number and the turbulent flow proper-ties, most influenced by the turbulent intensities and characteristic scales (Delnero *et al.,* 2005, 2012).

Dynamic stall is part of the unsteady separation phenomena associated with multiple flow field configurations. Non-stationary separation is one of the most important unsolved problems in fluid mechanics, in particular for turbulent flow conditions. Choundry *et al*. (2014) described the phenomena as: "Dynamic stall can be considered as the delay of conventional flow separation on wings and airfoils caused by rapid variations in the angle of attack beyond the critical static stall angle

due to virtually any kind of unsteady motion." The interest in achieving a better understanding of these phenomena comes from the many fields of application including air-crafts, helicopters, turbines, compressors, flow through pipes, turbulence generating devices and wind turbines blades (Volino and Hultgren, 2001).

The use of devices along the leading edge and on the upper surface of the airfoil, such as vortex generators, turbulators and other devices, affect the airfoils stall both statically and dynamically (Heine *et al*., 2013). At low Reynolds numbers in a quasi-laminar flow or at low turbulence intensity, an oscillating airfoil generates a fairly well defined flow pattern (Rudmin *et al*., 2013), based on the starting vortex. Some authors studied the separation phenomenon in wind turbine blade airfoils, obtaining loads and a description of the starting vortex (Wang *et al.,* 2010). Numerical Analysis at very low Reynolds numbers shows that sudden changes in angles of attack generate an important increment in lift. They also show a significant difference in the evolution of vortex shedding generated by the airfoil, which modify lift and drag loads (Larsen *et al*., 2007). Other studies also combine different systems, such as variations in the leading and trailing (flaps, Gurney flaps), which considerably modify the air-foil stall, generating different flow patterns in the dynamic stall, which these mechanisms are designed to control (Gharaki and Johnson, 2013).

Regarding this characteristic phenomenon of the airfoils, the concept can be developed to explain in detail the flow field pattern produced by this particular dynamic effect. Starting from large angles of attack with still attached flow, as the incidence angle continues to increase, a short recirculation bubble begins to appear on the airfoil leading edge (Sharma and Poddar, 2010). While this recirculating pattern is small, no significant deviations from the linear relationship of the lift vs. angle of attack will be produced. But for sufficiently large angles of attack, with an increasing recirculation bubble size, the flow separation process will begin and might lead to an abrupt or soft stall as was mentioned above.

When the incident flow of an airfoil changes rapidly to a sufficiently large angle of attack, dynamic stall may happen. Different types of stall have been identified in the past (Wandon *et al.*, 2006; Amromin, 2013). Most of recent studies are focused on the type of stall which occurs at high Reynolds numbers in the region located on the leading edge of modern thin airfoil (Yarusevich *et al*., 2006).

This work experimentally analyzes the effect known as dynamic stall on an airfoil under conditions of incident turbulent flow. In this case, the tests were made with a Wortmann FX 63-137 airfoil, commonly used in wind turbine blades. The choice of this airfoil is because in wind turbines under operation, due to changes in the incident flow, variation in the angle of attack during one revolution (velocity composition), interference of the tower, etc. the airfoils angle of attack changes and could experience a dynamic stall phenomenon. This effect is of big importance in the structural and performance design, then, it is relevant to have a good understanding of the aerodynamics that involves, the main motivation of this work.

The principal objective of this work is to determine the general fluid dynamic configuration of the airfoil's dynamic stall. The aim is to study the flow pattern, focusing on the process of bubble formation and separation in operating and stall conditions.

In order to reach the objective, the flow configuration around an airfoil in two different scenarios was studied. The first one, an intensive study of the static stall phenomena. The second scenario is the study of the stationary flow configuration, after a sudden change in the angle of attack, called as "dynamic case" in this work. Comparison of the two scenarios were made to understand the differences or similarities in the flow field.

II. METHODS

A. General

To meet the proposed objective, wind tunnel experimental studies on an airfoil powered with an electropneumatic system that allows quick-changes in the angle of attack were made. Also, the drive and control system of this mechanism was constructed in such a way to get different possibilities with the purpose of varying the angle of attack. Static loads, different visualization methods, and instantaneous velocity measurements taken up-stream, on the upper surface and wake of the airfoil, were made to analyze the dynamic behavior. Data was processed to explain the phenomena involved.

The instantaneous velocities acquired with a CTA (Constant Temperature Anemometer) system at the locations showed in Fig. 1 were plotted and analyzed. A PSD (Power Spectra Density) calculation was performed, for the same tests, in order to find predominant events in the flow field. From the analysis of the autocorrelation coefficients (Eq. 2) the temporal and spatial integral scales were calculated and compared between the static and the static after a sudden change (called dynamic in this work) to find some differences. The autocorrelation function (Eq. 1), its coefficient (Eq. 2) and the scales (Eq. 4) are explained in the next equations:

$$R_{u'}(\Delta t) = \lim_{T\to\infty} \int_0^T u'(t) \cdot u'(t+\Delta t) \cdot dt \,, \tag{1}$$

$$C(\Delta t) = \frac{R_{u'}(\Delta t)}{\sigma_{u'}^2} \,, \tag{2}$$

where

$$\sigma_{u'}^2 = \lim_{T\to\infty} \frac{1}{T} \int_0^T u'^2(t) \cdot dt \,, \tag{3}$$

is the variance. The autocorrelation coefficient function takes the unity value at the starting time, when the acquisition starts, and tends to zero when the time interval goes to infinity.

The time gap between starting time, and the time when the autocorrelation coefficient reaches the 1/*e* value for the first time, gives the comparative information about the integral time scale (λ_t). With this value, and the mean velocity (V) of the flow in the component ana-

lyzed, the spatial integral turbulent scale can be obtained using the Eq. 4.

$$\lambda_S = V\lambda_t . \quad (4)$$

Additionally, the turbulence intensity (*Ti*) was calculated for the same tests as:

$$Ti_u = \frac{\sigma_{u'}}{V}; \quad Ti_v = \frac{\sigma_{v'}}{V} . \quad (5)$$

A wavelet analysis was employed to determine the turbulent structures, applying the second derivative of the Gaussian ("Mexican Hat") as a wavelet mother.

$$(W_f)(b,a) = \frac{1}{\sqrt{a}} \int_{-\infty}^{\infty} f(t)\Psi\left(\frac{t-b}{a}\right) \cdot dt \quad (6)$$

where W_f is the wavelet transformation, $f(t)$ is the function to analyze (the velocity fluctuation in our case), and Ψ is the wavelet mother (Farge, 1990).

B. Facility and Test Conditions

The tests were conducted in the wind tunnel of the UIDET-LaCLyFA at the National University of La Plata (Delnero *et al*., 2012). It is a closed-circuit wind tunnel, with a test section of 1.4 m x 1.0 m x 7.5 m and V_{max} = 20 m/s. From a FX 63-137 Worthmann airfoil, a fiber-glass model was built with a 0.75 m span and a 0.25 m chord. A two end-plates arrangement was adopted in the tunnel model (Fig. 1) to produce a 2D flow field around the model. These end-plates were made by a symmetrical airfoil with variable rear flap and a NACA 0009 leading edge, to get a bi-dimensional flow across the test section of the wind tunnel.

First, a characterization of the airfoils loads was achieved by static test with a two components aerodynamic balance at different Reynolds numbers (102,000; 136,000 and 187,000; corresponding to a reference velocity of 6, 8 and 11 m/s, respectively, regarding the model chord length). These loads were taken at different angles of attack in order to obtain the aerodynamic lift coefficients vs angle of attack using the conventional equation

$$C_l = \frac{2L}{\rho V^2 C} . \quad (7)$$

The test was performed at an incident flow turbulent intensity of 1.8% in the longitudinal flow velocity, at the model height. Figure 2 shows the vertical turbulent

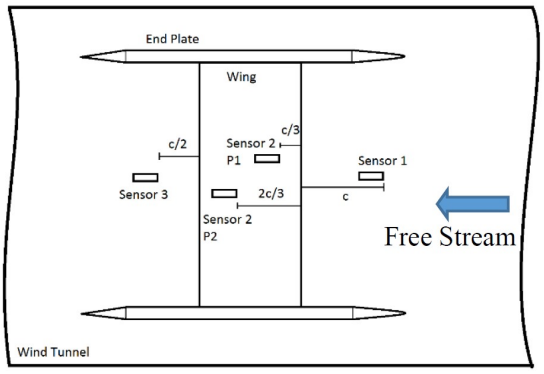

Figure 1. Wind Tunnel Setup

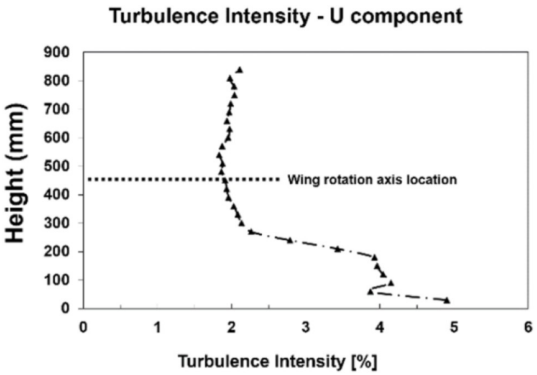

Figure 2. Vertical Distribution of the Turbulent Intensity for the longitudinal velocity component.

intensity distribution and the location of the model in this pro-file. Using the Taylor's frozen flow theory (Taylor, 1938), the integral temporal turbulent scale (λ_t) of the free stream takes the value of 0.11 seconds considering the first zero value criterion. However, if the exponential decrement criterion is used, the integral temporal turbulent scale (λ_t) is of 0.01 seconds. In all our tests, this situation remains invariable for the different configurations analyzed.

Measurement of the instantaneous velocity field was performed using a hot wire anemometry system (CTA Dantec Streamline), with a dual sensor (fiber film probes 55R51). The acquisition was made at a sample frequency of 2 kHz, using a low-pass band filter at 1 kHz, acquiring 16,384 samples in each test.

A mechanism was designed for an abrupt change in the angle of attack by means of an electro-pneumatic system. The mechanism consists of a double-acting piston, a solenoid valve controller, an air compressor, two limit sensors and a lever arm. System control was managed through a National Instruments USB Multifunction DAQ with associated software. It allowed the regulation of the change of angle of attack rate and its limits.

Then, a qualitative characterization of the airfoil stall in static conditions was made using different flow visualization techniques. Tufts on the airfoil and in its wake, and a suspension of heavy magnesium oxide in pure kerosene were granted to mark the stream lines on the airfoil after kerosene evaporation. For the different techniques, videos were recorded and high definition photographs were obtained. These visualizations were also performed for the cases of sudden change of angle of attack with the same methods mentioned above for the static stall case.

From the preliminary results of visualization tests, hot-wire anemometry measurements were made, placing the sensors in strategic areas identified in the visualization tests in order to find differences between static and dynamic conditions. Measurements were taken from the fluctuating components of the velocity at four fixed locations for all the tests: half-chord length downstream (Sensor 3) and a chord length upstream (Sensor 1 - wind tunnel reference) of the airfoil at the height of the airfoil rotation axis. Also, on the airfoil in two positions were

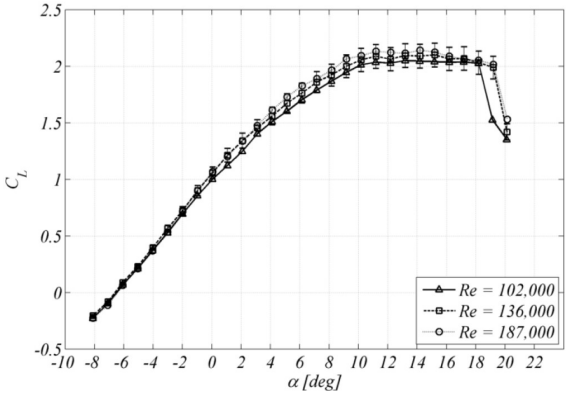

Figure 3. Lift coefficient versus angle of attack. Values corrected using the standard methods.

placed: at 1/3 (P1) and 2/3 (P2) (Sensor 2) of the chord length from the leading edge on the upper surface (Fig. 1). The last two sensors had a separation from the surface of 4 mm and are fixed together with the airfoil, moving as a whole. A detailed description and analysis of the fluid dynamic pattern was obtained.

III. RESULTS

A. Load tests (static)

With the study conducted with the load cells (aerodynamic balance), a calculation of the lift coefficient (C_l) using the Eq. 7, considering the corresponding corrections for tests in wind tunnels from Barlow *et al.* (1999), was made. Figure 3 shows the lift coefficient ver-sus angle of attack with its associated standard deviation. It can be seen in that figure a linear behavior from -8° to 2° of the C_l with respect to the angle of attack. However, the lift continues to increase monotonically up to 10° of the angle of attack. From that point, flow detachments in the trailing-edge starting the stall mechanism that ends at 18°, where a sharp drop given by the complete stall of the airfoil happened. Remarkably, the values of angle of attack are coherent to the experimental results of this airfoil for the same Reynolds number with laminar incident flow from Selig *et al*. (1995). The zero-lift, static stall and sharp drop on the lift coefficient angle of attack, are very close with the ones in the reference, but some difference was found in the maximum value of the lift coefficient.

This difference could be due to the high turbulence of the incident flow that lies in the results when compared with the laminar incident flows. Other author (Cao, 2010) made various tests to understand the effects of the different incident turbulence on the aerodynamic loads and on the flow field around the airfoil. The results shown by this author, states that an increase in the turbulence intensity produces a delay in the stall, an increase in the drag coefficient and an increase in the maximum lift coefficient. Also, Cao (2010) said in his work that with an increment in the turbulence scales (at constant intensity), the stall occurs at a lesser angle of attack and generates an increment on the lift and drag coefficient. That is the reason why the results showed in this work could differ in the maximum lift coefficient when is compared with other tests made for laminar flows.

In this airfoil, at these low Reynolds numbers, a bubble in the leading edge is generated when the angle of attack is bigger than 8°. In the "dynamic" cases, the angle of attack increases, and the bubble increases it size and moves to the trailing edge until the bubble explodes causing the total stall. In the stationary case, for a constant angle of attack, the bubble stay fixed at the leading edge modifying the flow structure around the airfoil. In general, this bubble generates an increment of the thickness of the shear layers that produces more lift and drag. For the detached flow, without total stall, a flow will be generated around this bubble that changes its configuration until it stabilizes in this new configuration. The flow over this bubble will be distorted for the adverse pressure gradient that generates the vortex shedding.

Using these results, an angle of start at 10° and a final of 24° was set to the dynamic tests. The 10° was selected to start the change in an angle of attack when the airfoil is in a partial stall, or in the very beginning of the stall; the final angle corresponded to the minimum determined by the sensibility and precision of the mechanism (sensor response and pneumatic effects).

B. Visualizations

Using the magnesium oxide visualization technique, the results showed streamlines and possible separation zones on the airfoil surface. This methodology is easy to implement and is capable to capture the evolution of the boundary layer (Genç *et al*., 2012). Visualizations were performed for different cases of static and dynamic stall conditions, at a unique rate of change on the angle of attack and at different Reynolds numbers.

The results of the paint method used in the wing showed a concordance to the stall condition, up to 8° angle of attack. A transition is also observed at the leading edge, differentiating the two types of sediment left by the paint. No separation in the trailing edge can be seen (Fig. 4a and Fig. 5a).

When the angle of attack is increased to 13°, areas of detached flow begin to emerge on the trailing edge and a well-marked bubble arises on the leading edge (Fig. 4b and Fig. 5b). This feature is enhanced as the angle of attack is increased, up to the complete stall of the airfoil in agreement with the load test. The observed flow at the trailing edge is characteristic of two-dimensional airfoil visualizations.

When this technique is applied to the dynamic test, with the mechanism of abrupt change in the angle of attack, the solutions obtained come from the stationary flow field after the change in the angle of attack due to the longtime of drying. In these dynamic tests, different solutions were found for the flow pattern at each angle of attack. Figure 4c and d, and Fig. 5 c and d show the solutions observed at an angle of attack of 19° degrees, for the static and the dynamic case in the trailing and leading edge view, respectively.

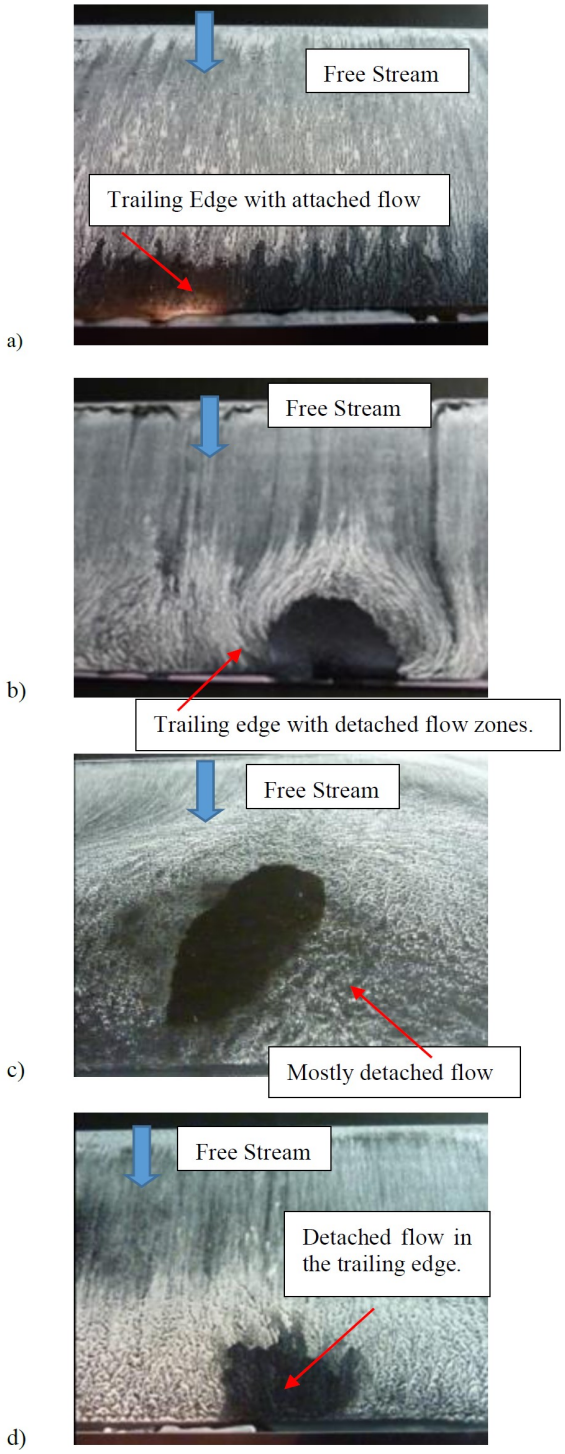

Figure 4. Flow visualization with paint at: $V = 11$ m/s; Trailing Edge view. a) $\alpha = 8°$, b) $\alpha = 13°$, c) $\alpha = 19°$, d) $\alpha = 10°$ to $19°$ (dynamic).

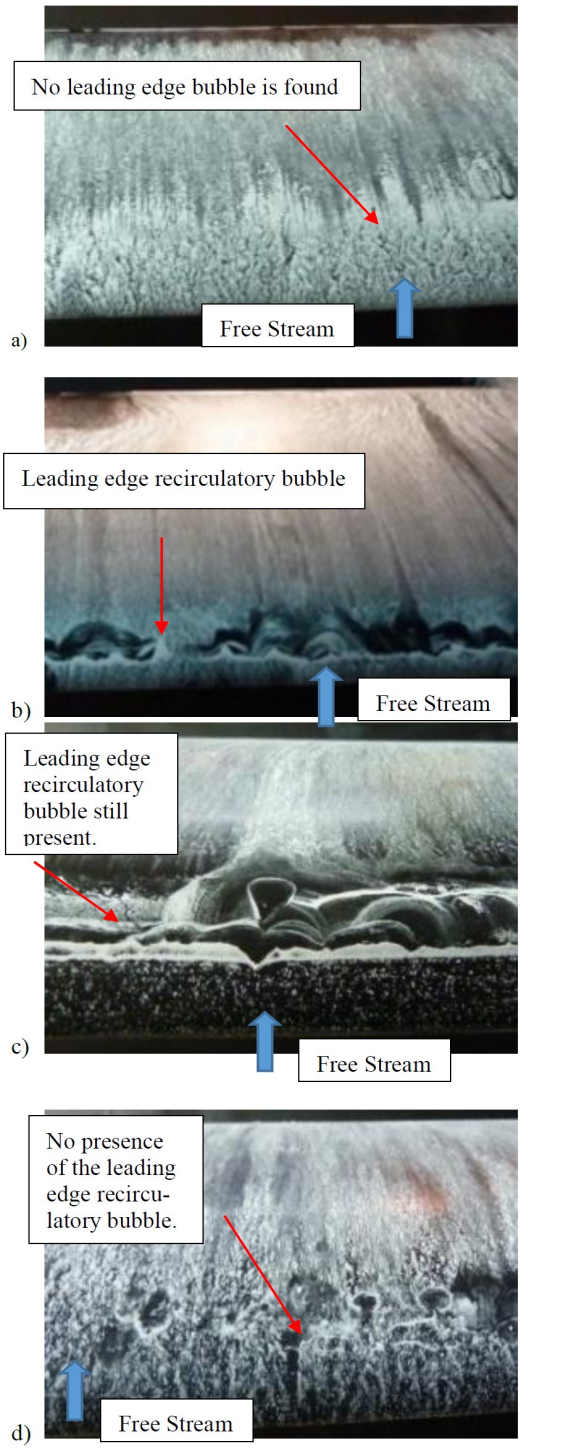

Figure 5. Flow visualization with paint at: $V = 11$ m/s; Leading Edge view. a) $\alpha = 8°$, b) $\alpha = 13°$, c) $\alpha = 19°$, d) $\alpha = 10°$ to $19°$ (dynamic).

The figures clearly show that in the static case a re-circulation bubble is present at the leading edge and a detachment zone from approximately half of the chord, whereas in the case of abrupt change from 10° to 19° degrees (dynamic case) the bubble does not appear and the detachment is observed at the trailing edge on the upper surface, delayed in comparison to the static case.

C. Hot-wire anemometry

From the analysis of the acquired data, different results are shown for the static stall case and for the stationary

part after the sudden change in the angle of attack (dynamic case). Results were produced for both longitudinal and vertical instantaneous velocities. Additional analyses including power density spectrums, turbulence intensities, autocorrelations (from which the information of spatial and temporal scales were obtained) and wavelets maps were performed.

Three sensors were located in order to measure the velocity component of the flow. Sensor 1 was a reference sensor (upstream of the model), sensor 2 was on the airfoil (in two positions on the upper surface) and sensor 3 was in the wake of the model.

The two static cases of analysis correspond with the static case at 10° and the static case at 24°. The "dynamic case" corresponds to the analysis of the stall at a 24° after a sudden change in the angle of attack starting the movement at 10°.

In the Fig. 6, Fig. 8 and Fig. 9, a vertical dotted black line shows the start of the change in the angle of the attack.

Sensor in the wake (Sensor 3)

Figure 6 shows a comparison of the velocities for the static cases at 10° and 24° of the angle of attack, and the abrupt change in the angle of attack (dynamic case). Instantaneous longitudinal (u) velocity components were acquired from the sensor in the wake of the airfoil.

With the aim of finding particularly events in the flow field, the power density spectrums of the signals were calculated. With this tool, it could be found detachments or periodical events generated by the airfoil that modify the flow field in the wake.

In Fig. 7, a power density spectrum analysis of the signals acquired in the wake's sensor for the static case at 24° is shown for the vertical velocity component. From that analysis, could be seen a peak at a specific frequency, which infers flow detachments from the airfoil. If the flow is attached to the airfoil surface, no spikes could be found in the PSD analysis (Delnero *et al.* 2011). A peak analysis was performed and the frequency detected is at 15 Hz.

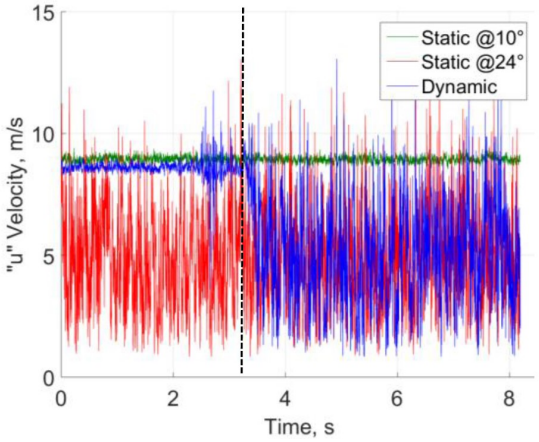

Figure 6. Longitudinal velocity component at the three study cases for: V = 8 m/s; α = 24° (red – static); α = 10° (green – static) and α = 10° to 24° (blue - dynamic). Sensor in the wake.

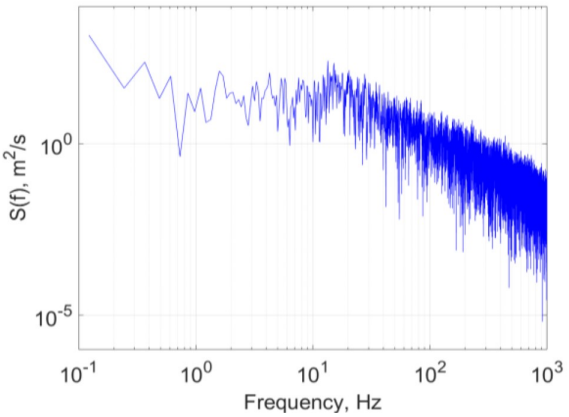

Figure 7. Vertical velocity component spectra for static stall at 24° in the wake at V = 8 m/s.

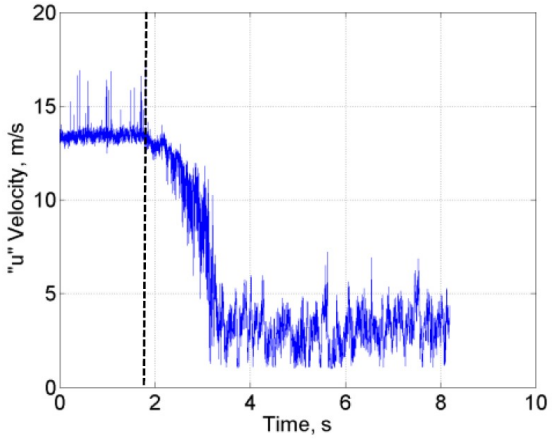

Figure 8. Longitudinal velocity components for the dynamic case at sensor 2 at P1 with V = 8 m/s.

Sensor on the wing (Sensor 2)

The figures described in this section show the results obtained from the data acquisition corresponding to the sensors placed on the wing, both for tests at static stall and at stall after a sudden change on the angle of attack. In Fig. 8 the instantaneous velocity component u can be seen. It can be easily observed when the change of angle of attack occurs. In Fig. 9 a comparison between two cases of static stall at different angles of attack and one dynamic case is shown. The objective of this comparison is to present the influence of the abrupt change in the angle of attack from a fixed angle of 10° up to 24°. For this reason, both static cases correspond to the initial and final state of the angle of attack.

In Fig. 10, it can be seen the PSD analysis for the vertical velocity component for the signals acquired on the airfoil on the Position 1 (1/3 of the chord length) for the dynamic and static cases. In this figure changes in the energies behavior are not noticeable when comparing the static and dynamic cases. This PSD results are frequently revealed when detached flow structures could not be detected for a characteristic frequency, or with a predominant frequency. Same result was found for the longitudinal velocity component.

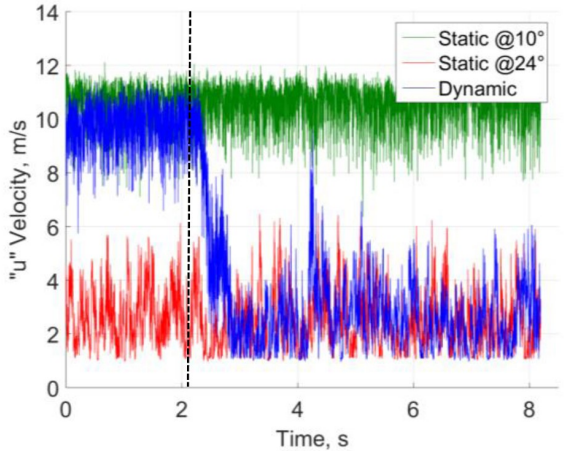

Figure 9. Longitudinal velocity component comparison between static at 10° (green) and 24° (red), and dynamic from 10° up to 24° (blue) for the sensor 2 at P2 with $V = 8$ m/s.

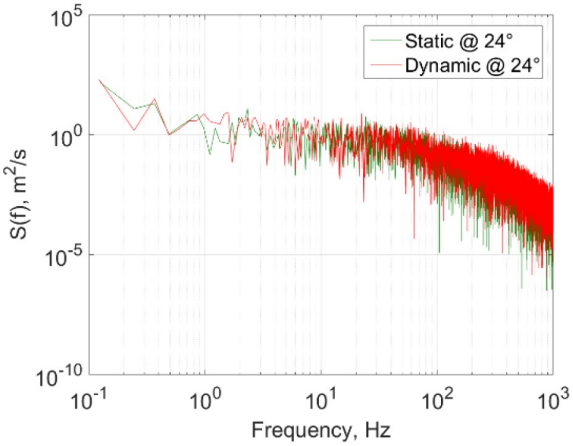

Figure 10. Vertical velocity component Spectra at Static at 24° (green) and dynamic (red) at 24° for the sensor 2 at P1 with $V = 8$ m/s.

Signal correlations

The previous analysis was followed by an analysis of the autocorrelation coefficients for the different cases, to determine under some criteria, temporal and spatial scales of turbulence in the flow measurement. Temporal correlations were also conducted for the results of the different sensors in order to find flow patterns or flow behaviors observed between the flow field on the airfoil and the flow field in the wake of it.

In Fig. 11 can be seen the autocorrelation coefficient for the 3 sensors (sensor 2 at P1) for the static case at 24°, and dynamic case at 24°, that is the stationary part of the signal at 24° after the sudden change in the angle of attack.

To determine the integral and spatial scales of the turbulence, the exponential decrement criteria was employed on the autocorrelation functions. In this analysis, using the frozen flow theory (Taylor, 1938), a comparison of the time when the function takes the $1/e$ value was performed, obtaining the time and spatial scales, using the mean velocity of each sensor for each test. This evaluation was managed for the three sensors in simultaneous and analysing both velocity components (u and v). In Fig. 11 it can be observed the analysis for the static and dynamic case at 24°. The analysis for all the signals were performed using the same signal lengths. As expected, important changes in the temporal scales of the sensor placed in the wing and wake were found, but not in the sensor of the incident flow. In Table 1 the values of the turbulence intensities for the static and dynamic cases at 24° are shown. In Table 2 and Table 3 summarized results from the autocorrelation coefficients are presented, to analyze the differences between temporal and spatial integral scales in the static and dynamic tests using the frozen flow theory.

Looking the results summarized in Table 2, it can be seen the differences in the spatial scales that generates the presence of the airfoil (flow vs. wake). The same effect is found in Table 3 analyzing the stationary case after the sudden change in the angle of attach (dynamic at 24°). In Table 1 we show the turbulent intensity values for the u velocity component in the static and dynamic case, for three specific positions (flow, wing P1 and wake). There can be observed the different conditions for each case (static and dynamic) related to the flow pattern behaviour.

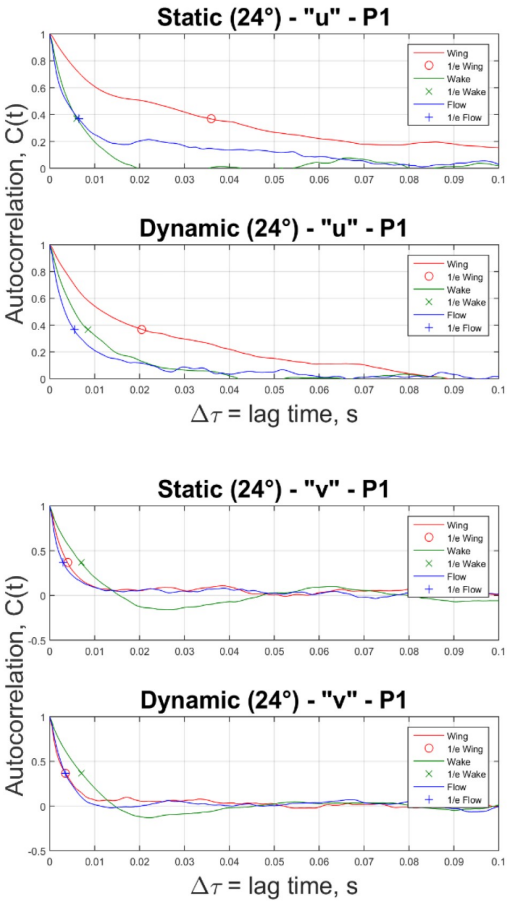

a)

b)

Figure 11. Autocorrelation for the 3 sensors with the sensor in the wing at P1 for the Static and Dynamic case at 24° with $V = 8$ m/s. a) Autocorrelation for the longitudinal velocity fluctuation. b) Autocorrelation for the vertical velocity fluctuation.

Table 1. Turbulence intensity for the *u* component

Turbulence Intensity		
	Static	Dynamic
Flow	2.04%	1.90%
Wing (P1)	42.71%	33.37%
Wake	38.73%	39.18%

Table 2. Temporal and Spatial Scales from autocorrela-tion coefficients. Static Case at 24°

Static Case 24°				
Place	Vel. Comp	Temporal Scale [s]	Mean Vel.[m/s]	Spatial Scale[m]
Flow	*u*	0.006	7.421	0.044000
	v	0.003	-0.402	0.001200
Wing P1	*u*	0.036	2.347	0.070000
	v	0.004	-0.210	0.000084
Wing P2	*u*	0.015	2.458	0.036800
	v	0.003	-0.178	0.000534
Wake	*u*	0.006	4.607	0.027600
	v	0.008	0.527	0.004216

Table 3. Temporal and Spatial Scales from autocorrela-tion coefficients. Dynamic Case at 24°

Static Case 24°				
Place	Vel. Comp	Temporal Scale [s]	Mean Vel.[m/s]	Spatial Scale[m]
Flow	*u*	0.008	5.008	0.04010
	v	0.003	2.095	0.00628
Wing P1	*u*	0.021	3.053	0.06410
	v	0.003	-0.254	0.00076
Wing P2	*u*	0.023	2.698	0.06205
	v	0.002	-0.215	0.00043
Wake	*u*	0.021	2.709	0.05689
	v	0.002	-0.180	0.00036

If a comparison in the wake sensor is performed between static and dynamic case, in the dynamic case, the u spatial scale is the double of the same in the static case, and com-paring the v component, in the dynamic case is an order of magnitude smaller with similar conditions in the incident flow. These differences, between the two tested cases, in the turbulent scales expose changes in the turbulent structures in the wake flow field. These changes are independent of the velocity and energy involved. Is known that could be found in a turbulent flow the same velocity and turbulent intensity with different integral temporal scales.

For a better understanding of these phenomena, a frequency and time analysis was performed using the wavelet technique.

Wavelet Analysis

A wavelet analysis of the signals in both components was performed to characterize the vortices found in the different sensors and, to make a comparison between the results of the different cases (static and dynamic). In Fig. 12 the results of the wavelet maps for the vertical component of the velocity in the three sensors are shown for the static and dynamic case.

In these figures, the time scales of the wavelets (correlated with the signals) is represented versus the signal time, both expressed in seconds. For this analysis, 512 time scales of the wavelet were used. The color plots in

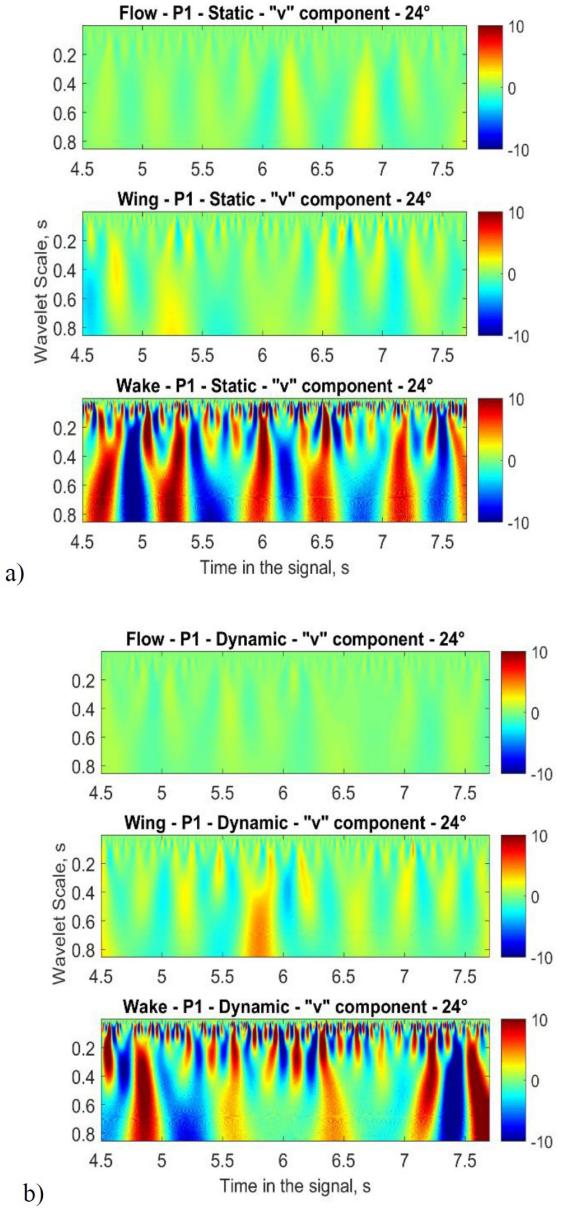

Figure 12. Wavelets analysis for the vertical velocity component of the three sensors at $V = 8$ m/s. a) Static case at 24°. b) Dynamic case at 24° (static after sudden change).

these images represent the wavelet coefficients where a maximum value stands for a better matching between the wavelet used (second Gaussian derivative) at that specific wavelet time scale and signal time. More information about this technique used for this analysis could be found in Farge (1990).

In the full detached flow test (24°), in both cases, the high frequencies events which means small size vortices detached from the airfoil surface into the wake, had a temporal wavelet scale lesser than 0.3 s. If the low frequencies are analyzed (bigger than 0.3 s), differences between the static and dynamic case are exposed. In the static case, the low frequencies had a similar importance than the high frequencies, while in the dynamic case, in

the wavelet map could be seen small importance of the low frequencies (low matching between the wavelet at that scales and the signal). These results reveal the formation of different wake patterns for the static and dynamic case in complete stall. That enhances the hypothesis of different flow patterns in a static stall versus a dynamic stall.

IV. DISCUSSION

For the study of the airfoil stall in turbulent flow, visualization tests, aerodynamic load test and hot-wire anemometry measurements were performed. As previously showed, significant differences in the visualization with magnesium oxide between static stall and dynamic stall cases were found.

The flow pattern found on the airfoil for a static stall condition (e.g., 19° angle of attack) differs remarkably from the flow pattern for the abrupt angle of attack change condition from 10° to 19°. For the static condition, a significant recirculation bubble arises on the leading edge, but while performing the abrupt change of angle of attack, that bubble is quite smaller, and can be swept by the sudden movements. This reveals the different flow patterns for an airfoil in stall conditions.

Moreover, by this technique different types of flow are observed behind the area of the leading edge above the airfoil upper surface. This makes a different airfoil flow circulation, and therefore, a different fluid dynamic configuration in both cases.

In order to explain such behavior, hot-wire anemometry tests were performed placing dual sensors (two components) upstream, on the airfoil (in two positions) and in the wake of the airfoil, thus, intended to analyze the flow behavior under these conditions.

From the analysis of the acquired signals with the hot-wire anemometers, the behavior of the flow before, during and after the sudden change in the angle of attack, could be seen. Important differences in the mean velocities and turbulence intensities were not found in both components when were compared.

In the analysis of the density power spectrums of the signals, differences in the energies over the wing comparing the static and dynamic cases were not found. However, small peaks were detected in low frequencies in the wake sensor that could be generated by detached flow over the wing for these angles of study.

Significant differences were noticed analyzing the auto-correlation of the signals in all the sensors. For these cases, differences in the spatial and temporal integral scales of the turbulence were found over the airfoils wake. The same differences were identified from the wavelets map, where the energies show different structures with different turbulence associated. Different events, with different time and intensity magnitude, could be found in the wake.

Is known that this airfoil in low Reynolds number flows develops a leading edge bubble which increases it size with the angle of attack increment. Under turbulent flows, the bubble also exists but is not capable of movement as in a laminar flow. The results found, suggest that the bubble development is altered by the detached flow in the transition of the movement after a quick change in the angle of attack. Arriving at the stationary scenario, after the movement, we suggest that the flow field is different compared with the obtained after a statically movement.

Using these results as a base, new tests will be performed with the aim of get a better understanding of this fluid-dynamic phenomenon. These tests involve hot-wire measurements in more points of the boundary layer to detect the evolution of it and surface pressure measurements. All the results are shown for the 8 m/s free stream velocity due to similar results found at the other reference velocities. So, in the low Reynolds number regime, the Reynolds number variation does not make a considerable influence in the phenomena explained.

V. CONCLUSIONS

Tuft techniques and the injection of smoke showed no significant results on the emergence of the phenomenon of dynamic stall, but considerable results were found in the general configuration of the static stall. However, interesting results were detected in both cases using the painting technique with kerosene and magnesium oxide.

Based on the visualizations, other authors publications and the results of the hot-wire anemometry measurements on the airfoil in turbulent flow conditions with a quick angle of attack change, the authors suggest, after all the analysis made (mean velocities and its fluctuations, turbulence intensities, time and spatial integral scales, PSD and wavelets), the presence of differences in the fluid-dynamic structures generated on the wake when the airfoil is at 24° in a static case, with respect to the stationary part of the airfoil at 24° after a sudden change in the angle of attack. As was mentioned in the Discussion section, more tests are needed to confirm these differences and validate these results.

ACKNOWLEDGEMENTS

This work is supported by CONICET (Consejo Nacional de Investigaciones Científicas y Técnicas, Argentina – Technical and Scientific Research National Council).

REFERENCES

Amromin, E.L., "Analysis of the Airfoil Stall with a Modification of Viscous-Inviscid Interaction Concept," *ASME J. Fluids Eng.*, **135**, 051105-051105-7 (2013).

Barlow, J.B., W.H. Rae and A. Pope, *Low Speed Wind Tunnel Testing*, 2nd ed., John Wiley & Sons, New York (1999).

Cao, N, *Effects of turbulence intensity and integral length scale on an asymmetric at low Reynolds number,* Master Thesis, the University of Windsor, Ontario, Canada (2010).

Choundry, A., R. Leknys, M. Arjomandi and R. Kelso, "An insight into the dynamic stall lift characteristics," *Experimental Thermal and Fluid Science*, **58**, 188-208 (2014).

Delnero, J.S., J. Marañón Di Leo, F. Bacchi, J. Colman and U. Boldes, "Experimental determination of the

influence of Turbulent scale on the lift and drag coefficients of Low Reynolds number airfoils,". *Latin American Applied Research,* **35,** 183-188, (2005).

Delnero, J.S., J. Marañón Di Leo, M., Camocardi , M. Martinez and J. Colman, "Experimental study of vortex generators effects on low Reynolds number air-foils in turbulent flow," *Int. J. Aerodynamics,* **2**, 50-65(2012).

Elkhoury, M., J. Najem and Z. Nakad, "URANS Modeling of Three Airfoils with Different Stall Mechanisms." *Proc. ASME. 48401*, **1**, 795-800 (2008).

Farge, M., "Transformee en ondelettes continue et application a la turbulence," *Journ. Annu. Soc. Math.*, France, 17-62 (1990).

Genc, M.S., I. Karasu and H.H. Acikel, "An experimental study on aerodynamics of NACA2415 aerofoil at low Re numbers," *Experimental Thermal and Fluid Science*, **39**, 252–264 (2012).

Gharali, K. and D.A. Johnson, "Dynamic stall simulation of a pitching airfoil under unsteady freestream velocity," *Journal of Fluids and Structures*, **42,** 228–244 (2013).

Heine, B., K. Mulleners, G. Joubert and M. Raffel, "Dynamic Stall Control by Passive Disturbance Generators," *AIAA Journal*, **51**, 2086-2097 (2013).

Hui, H. and Y. Zifeng, "An Experimental Study of the Laminar Flow Separation on a Low-Reynolds-Number Airfoil," *ASME Journal of Fluids Engineering*, **130**, 1-11 (2008).

Larsen, J.W., S.R.K. Nielsen and S. Krenk, "Dynamic stall model for wind turbine airfoils," *Journal of Fluids and Structures,* **23**, 959–982 (2007).

Rudmin, D., A. Benaissa and D. Poirel, "Detection of Laminar Flow Separation and Transition on a NACA-0012 Airfoil Using Surface Hot-Films," *ASME Journal of Fluids Engineering*, **135**, 101104-101104-6 (2013).

Selig, M.S., J.J. Guglielmo, A.P. Broeren and P. Giguère, *Summary of Low-Speed Airfoil Data*, **I**, 1st ed., SoarTech Publications, Virginia Beach, Virginia (1995).

Sharma, D.M. and K. Poddar, "Experimental Investigations of Laminar Separation Bubble for a Flow past an Airfoil," *Proc. ASME: Structures and Dynamics*, Parts A and B, **6,** 1167-1173 (2010).

Taylor, G.I., "The Spectrum of Turbulence," *Proceedings of the Royal Society a Mathematical, Physical and Engineering Sciences,* **164**, 476-490 (1938).

Volino, R.J. and L.S. Hultgren, "Measurements in Separated and Transitional Boundary Layers Under Low-Pressure Turbine Airfoil Conditions," *ASME J. Turbomach*, **123**, 189–197 (2001).

Wandon, J., L. Bo-Sung, Y. Kwanjung and L. Dong-Ho, "Combining Passive Control Method for Dynamic Stall Control," *Journal of Aircraft,* **43**, 1120-1128 (2006)

Wang, S., L. Ma, D. Ingham, M. Pourkashanian and Z. Tao, "Numerical investigations on dynamic stall of low Reynolds number flow around oscillating airfoils," *Computers and Fluids*, **39**, 1529–1541, (2010).

Yarusevych, S., J.G. Kawall and P.E. Sullivan, "Airfoil Performance at Low Reynolds Numbers in the Presence of Periodic Disturbances," *ASME Journal of Fluids Engineering*, **128**, 587-595 (2006).